Fig. 5. Two possible environments for the UO$_2^{2+}$ unit in the conduction plane.

local situation may be on the basis of occupations and electrostatic considerations. The two distinctly different environments for the UO$_2^{2+}$ ions suggested by the optical spectrum are likely to be those with and without Na$^+$ as a nearest neighbour (see Fig. 5). There can be several sources for the lack of homogeneity associated with a given site, e.g., the UO$_2^{2+}$ ion can be slightly tilted, it can be influenced by next-nearest-neighbour Na$^+$ ions, or a second uranyl ion can occupy a nearby site. It is clear, however,

that the structural picture presented here is fully consistent with the appearance of the luminescence spectrum.

References

BECKER, P. J. & COPPENS, P. (1974). *Acta Cryst.* A30, 129–147.
BETTMAN, M. & PETERS, C. R. (1969). *J. Phys. Chem.* 73, 1774–1780.
BRIANT, J. L. & FARRINGTON, G. C. (1980). *J. Solid State Chem.* 33, 385–390.
BRITTAIN, H. G. & PERRY, D. L. (1980). *J. Phys. Chem.* 84, 2630–2634.
DUNN, B., FARRINGTON, G. C. & THOMAS, J. O. (1989). *Mater. Sci. Bull.* 14(9), 22–30.
HOLLINGSWORTH, G., ZINK, J. I., BARRIE, J. D. & DUNN, B. (1987). *J. Am. Chem. Soc.* 109, 6849–6851.
LEHMANN, M. & LARSEN, F. K. (1974). *Acta Cryst.* A30, 580–584.
LUNDGREN, J.-O. (1982). *Crystallographic Computer Programs.* Report UUIC-B13-04-05. Institute of Chemistry, Univ. of Uppsala, Sweden.
REISFELT, R., EYAL, M. & JØRGENSEN, C. K. (1986). *Chem. Phys. Lett.* 132, 252–255.
THOMAS, J. O. (1992). *Solid State Ion.* 53–55, 1311–1316.

Modulation Wave Approach to the Structural Parameterization and Rietveld Refinement of Low Carnegieite

BY RAY L. WITHERS* AND JOHN G. THOMPSON

Research School of Chemistry, Australian National University, Canberra, ACT 0200, Australia

Abstract

The crystal structure of low carnegieite, NaAlSiO$_4$ [M_r = 142.05, orthorhombic, $Pb2_1a$, a = 10.261(1), b = 14.030(2), c = 5.1566(6) Å, D_x = 2.542 g cm^{-3}, Z = 4, Cu $K\alpha_1$, λ = 1.5406 Å, μ = 77.52 cm^{-1}, $F(000)$ = 559.85], is determined *via* Rietveld refinement from powder data, R_p = 0.057, R_{wp} = 0.076, R_{Bragg} = 0.050. Given that there are far too many parameters to be determined *via* unconstrained Rietveld refinement, a group theoretical or modulation wave approach is used in order to parameterize the structural deviation of low carnegieite from its underlying C9 aristotype. Appropri- ate crystal chemical constraints are applied in order to provide two distinct plausible starting models for the structure of the aluminosilicate framework. The correct starting model for the aluminosilicate framework as well as the ordering and positions of the non-framework Na atoms are then determined *via* Rietveld refinement. At all stages, chemical plausibility is checked *via* the use of the bond-length-bond-valence formalism. The JCPDS file number for low carnegieite is 44-1496.

1. Introduction

Carnegieite, NaAlSiO$_4$, is one of a large family of materials topologically closely related to the so-called C9 structure type (O'Keeffe & Hyde, 1976). Its parent

---

* Author to whom all correspondence should be addressed.

crystal structure can be described as a 'stuffed' derivative of the C9 structure type in which half the cavities in the corner-connected tetrahedral $AlSiO_4$ framework are filled with Na atoms (see Fig. 1). It exists as the stable polymorph of $NaAlSiO_4$ between 1523 K and its melting point at 1799 K. Early work on high carnegieite determined that it had a cubic structure with space-group symmetry $P2_13$ or $F\bar{4}3m$ and cubic unit-cell dimension of 7.37 Å. Upon cooling relatively quickly to room temperature, high carnegieite undergoes a reversible displacive structural phase transition at 940 K to low carnegieite (Klingenberg & Felsche, 1981).

The crystal structure of low carnegieite has not been solved. Indeed even its unit-cell and space-group symmetry have proved difficult to determine owing to the extremely sluggish kinetics of formation of fully ordered, single-phase low carnegieite from the component oxides. Such sluggish kinetics in conjunction with the above structural phase transition rule out single-crystal growth and mean that synthetic powder preparations have almost invariably been multiphase, including several phases which are also closely related to the C9 structure type. With sufficient homogenization of the component oxides in conjunction with annealing at 1673 K, it has recently proved possible to prepare powder specimens in which the only crystalline phase present was low carnegieite, although even this material was found to contain some 30–50% of a glass phase (Thompson, Withers, Whittaker, Traill & Fitz Gerald, 1993).
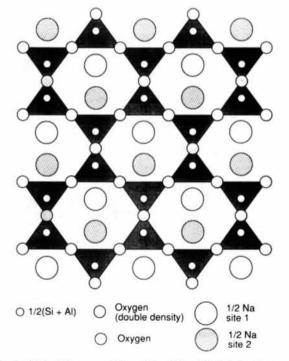

Fig. 1. Polyhedral representation of the $Fd3m$ C9-related aristotype of low carnegieite projected along a cubic $\langle 110 \rangle$ direction.

Legend:
○ 1/2(Si + Al)   ○ Oxygen (double density)   ◯ 1/2 Na site 1
                  ○ Oxygen   ◯ 1/2 Na site 2

Electron microprobe analysis of this crystalline phase confirmed the stoichiometry to be $NaAlSiO_4$ while examination by X-ray powder diffraction, TEM and solid-state NMR gave an orthorhombic unit cell $a' = 10.261$, $b' = 14.030$ and $c' = 5.1566$ Å with space-group symmetry $Pb2_1a$ (non-standard setting of $Pca2_1$). This cell setting was chosen so as to be directly comparable to that reported for what appears to be a closely related material, namely $Na_4Mg_2Si_3O_{10}$ (Shannon, 1979; Foris, Zumsteg & Shannon, 1979). In addition to the similarity of their powder XRD traces, $Na_4Mg_2Si_3O_{10}$, like carnegieite, also undergoes a high-temperature cubic to orthorhombic phase transition at ~900 K. $KGaO_2$ is representative of a family of fully stuffed C9 derivative structures which also appear to be related in that they have similar cell dimensions and a related although higher space-group symmetry of $Pbca$ when the same cell setting is used (Vielhaber & Hoppe, 1969; Grey, Hoskins & Madsen, 1990).
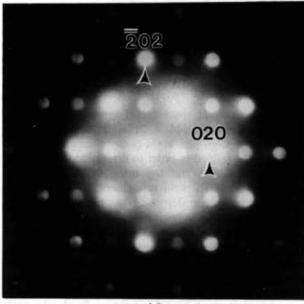
Given a resultant space-group symmetry of $Pb2_1a$, there are potentially $(14 + 2) \times 3 = 48$ displacive degrees of freedom plus eight compositional degrees of freedom to be refined in order to determine the structure of low carnegieite - far too many to be refined via an unconstrained Rietveld refinement. Therefore, it is essential to be able to derive a plausible starting model for the structure before beginning a Rietveld refinement.

In this paper, a group theoretical or modulation wave approach is used in order to parameterize the structural deviation of low carnegieite from its underlying C9 aristotype (Barnighausen, 1980, and references contained therein). Thereby the structural relationship between low carnegieite and its C9 aristotype is clearly spelt out. Appropriate crystal chemical constraints are then applied in order to provide two distinct plausible starting models for the structure of the aluminosilicate framework. The correct starting model for the aluminosilicate framework as well as the ordering and positions of the non-framework Na atoms is then determined via Rietveld refinement. At all stages, chemical plausibility is checked via the use of the bond-length–bond-valence formalism.

2. Modulation wave approach

Electron-diffraction patterns of low carnegieite, and indeed of all C9-related superstructures, display a subset of strong Bragg reflections (G_p) corresponding in essence to a (strain deformed) underlying $Fd3m$ C9-related parent structure (see Fig. 2) in addition to extra satellite reflections (at $G_p \pm q$) arising from the structural deviation or modulation of the fractional coordinates of the low carnegieite structure away from those of the C9-related parent structure. Infinite wavelength strain waves corresponding to a deformation of the original parent structure unit-cell parameters always accompany

such changes in fractional coordinates. In the case of low carnegieite, this strain deformation is a lattice-equivalent (Bärnighausen, 1980) transformation which lowers the isogonal point-group symmetry of the $C9$ parent structure from cubic $m3m$ to orthorhombic mmm.

The changes in fractional coordinates and occupancies of the resultant structure can now be described in terms of compositional and displacive modulation of the latter, strain deformed (reference) structure. Knowledge of the unit-cell and space-group symmetry of the resul-

tant structure enables the most general possible atomic displacement pattern compatible with each observed independent modulation wavevector $\mathbf{q}$ to be written down and hence defines the structural parameters which need to be determined in any structure refinement. Application of plausible crystal chemical constraints such as the requirement that the framework SiO_4 and AlO_4 tetrahedra be as regular as possible can then be used to see which resultant space-group symmetry-allowed parameters are likely to be small, to provide approximate relationships between formally independent structural parameters and in general to give a plausible starting model for the subsequent refinement.

2.1. C9 aristotype

The underlying parent structure or aristotype of low carnegieite has the same space-group symmetry as $C9$ itself, *i.e.* $Fd3m$ with one $NaAlSiO_4$ formula unit per primitive parent unit cell and with fractional coordinates given by: $M1$ at $0, 0, 0$; $M2$ at $\frac{1}{4}, \frac{1}{4}, \frac{1}{4}$; $Na1$ at $\frac{1}{2}, \frac{1}{2}, \frac{1}{2}$; $Na2$ at $\frac{3}{4}, \frac{3}{4}, \frac{3}{4}$; $O1$ at $\frac{1}{8}, \frac{1}{8}, \frac{1}{8}$; $O2$ at $\frac{1}{8}, -\frac{1}{8}, -\frac{1}{8}$; $O3$ at $-\frac{1}{8}, \frac{1}{8}, -\frac{1}{8}$; and $O4$ at $-\frac{1}{8}, -\frac{1}{8}, \frac{1}{8}$ plus the face-centring translations (see Fig. 3). The O-atom sites are always fully occupied while the average atomic scattering factors of the metal sites, denoted f_{M1}^{av}, f_{M2}^{av}, f_{Na1}^{av}, f_{Na2}^{av} are necessarily composition dependent *e.g.* for $NaAlSiO_4$, $f_{M1}^{av} = f_{M2}^{av} = \frac{1}{2}(f_{Al} + f_{Si})$; $f_{Na1}^{av} = f_{Na2}^{av} = \frac{1}{2}f_{Na}$. The eight compositional degrees of freedom referred to in the *Introduction* correspond to the determination of the occupancies of these cation sites in the resultant unit cell.
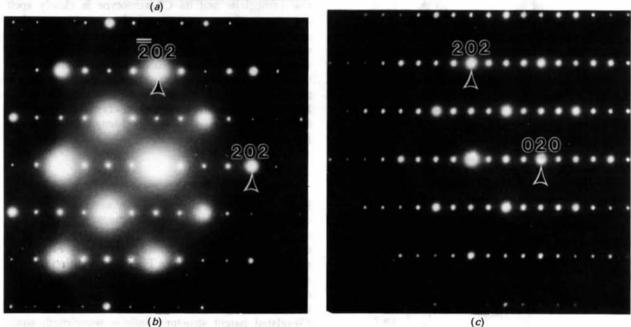
(a)

(b)

(c)

Fig. 2. (a) [100] = [101]$_{C9}$ zone-axis microdiffraction pattern, (b) an [010] = 2[010]$_{C9}$ zone-axis selected-area diffraction pattern (SADP) and (c) an [001] = [101]$_{C9}$ zone axis SADP of low carnegieite. The indexing is with respect to the $C9$ aristotype.

The unit-cell size to be associated with this idealized $C9$ aristotype can be determined *via* usage of the bond-length–bond-valence approach (see, for example, Brown & Altermatt, 1985; Brese & O'Keeffe, 1991) in conjunction with the reasonable assumption that the AlO_4 and SiO_4 tetrahedra remain as regular as possible. Ideal AlO_4 and SiO_4 tetrahedra have Al—O and Si—O tetrahedral distances given by 1.757 and 1.624 Å, respectively [determined *via* use of the bond-valence parameters given by Brese & O'Keeffe (1991)]. The corresponding oxygen–oxygen tetrahedral edge lengths within the AlO_4 and SiO_4 tetrahedra are given by 2.869 and 2.652 Å, respectively.

With such a tetrahedral framework, an ideal $C9$-type parent structure would have a cubic unit-cell parameter given by $4(1.757 + 1.624)/3^{1/2} = 7.808$ Å and an average oxygen–oxygen tetrahedral edge length of $7.808 \times 2^{1/2}/4 = 2.761$ Å. Using the bond-length–bond-valence formalism, an Na atom in either the Na1 or Na2 (initially 12-coordinate) truncated tetrahedral sites would have an apparent valence (AV) of only ~ 0.24, *i.e.* all such Na atoms would be heavily underbonded. Therefore, the structure needs to collapse *via* coupled rotations of the framework tetrahedra in such a way as to increase the AV of the Na atoms.

Note that the average structure of a $C9$-related superstructure such as low carnegieite (defined as the structure that would result if the amplitudes of the modulations associated with the satellite reflections $G_p \pm q$ all went to zero, *i.e.* the structure corresponding to the subset of strong Bragg reflections G_p alone) still will not be the same as the underlying aristotype or parent structure (Perez-Mato, Madariaga, Zuñiga & Garcia Arribas, 1987) defined above for two reasons. Firstly,
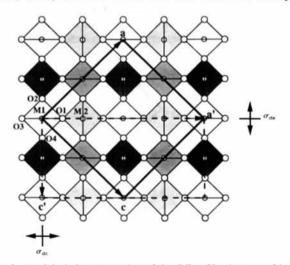

Fig. 3. A polyhedral representation of the $Fd3m$ $C9$ aristotype of low carnegieite projected along the $[010] = 2[010]_{C9}$ axis. The projected unit cell of the aristotype is given by the bold lines while that of the resultant structure is given by the dashed lines. The independent atoms per primitive unit cell of the $C9$ aristotype are labelled as are some relevant symmetry operations of the aristotype.

the possibility of $q = 0$ compositional and displacive modulation must be allowed for. Indeed, in the case of low carnegieite, solid-state NMR evidence requires each SiO_4 tetrahedra to be surrounded by four AlO_4 tetrahedra and *vice versa* (Thompson *et al.*, 1993). Such tetrahedral cation ordering destroys any possibility of an inversion centre in the resultant structure and can be described in terms of a $q = 0$ compositional modulation of the above aristotype. Such a $q = 0$ compositional modulation must, of necessity, be accompanied by a small amplitude $q = 0$ displacive modulation corresponding to a small amplitude shrinkage and expansion of the SiO_4 and AlO_4 tetrahedra, respectively, relative to the average tetrahedral size.

Even if the amplitude of this $q = 0$ mode was also put to zero, however, the resultant average structure or reference structure would still not be identical to the underlying aristotype defined above. The reason is the strain deformation of the original parent structure unit-cell parameters which also occurs at the phase transition. As mentioned above, in the case of low carnegieite, such strain deformation lowers the isogonal point-group symmetry of the $C9$ parent structure from $m3m$ to mmm, *i.e.* the point-group symmetry operations of the $C9$ aristotype which remain in the strain-deformed 'second generation' parent structure are given by $mmm = \{E,\ C_{2c},\ C_{2e},\ C_{2y},\ i,\ \sigma_{dc},\ \sigma_{de},\ \sigma_y\}$ [see Fig. 1.3 of Bradley & Cracknell (1972) and Fig. 3]. Formally the parent structure space-group symmetry is thereby lowered from $Fd3m$ (**a**, **b**, **c**) to $Immm$ $[\frac{1}{2}(\mathbf{a} + \mathbf{c}),\ \mathbf{b},\ \frac{1}{2}(-\mathbf{a} + \mathbf{c})]$ (see Fig. 3). This latter, strain-deformed parent structure represents a 'second generation' parent structure (or reference structure) from which the true structure can now be derived *via* appropriate compositional and displacive modulation. Note that the reference structure can be described in two superficially different but entirely equivalent manners. Firstly, as described above, *i.e.* $Immm$ $[\frac{1}{2}(\mathbf{a} + \mathbf{c}),\ \mathbf{b},\ \frac{1}{2}(-\mathbf{a} + \mathbf{c})]$. This, however, formally requires a different choice of parent cell parameters and hence of modulation wavevectors as defined below. Given that structural comparison with other $C9$-related superstructures is most direct if the same $C9$ parent cell is used, we have chosen to use the same cell parameters as for the $C9$ aristotype, *i.e.* **a**, **b**, **c** and F-centered, but to keep in mind that only space-group symmetry operations whose rotational component belongs to one of the mmm point-group symmetry operations defined above are relevant. Hence when considering little cogroups appropriate to various modulation wavevectors below, only those point-group symmetry operations belonging to the point-group symmetry mmm are taken into account.

2.2. *Structural deviation away from the $C9$ aristotype*

O'Keeffe & Hyde (1976) have shown how the major component of the structural deviation of low cristobalite

and β-NaFeO$_2$-type structures from their underlying C9 aristotypes can be described in terms of coupled rotations of virtually rigid framework tetrahedra around their $\bar{4}$ tetrahedral axes. Alternatively, and apparently equivalently, such structural deviation away from the underlying C9 aristotype can be described in terms of coupled rotations of the framework tetrahedra about orthogonal ($\langle 110 \rangle$ and $\langle 1\bar{1}0 \rangle$) tetrahedral edges. In a very real sense, rotation of the framework tetrahedra around their $\langle 110 \rangle$ tetrahedral edges is the natural 'normal mode' for such C9-related structures [see, for example, the diffuse scattering characteristic of both high and low cristobalite (Withers, Thompson & Welberry, 1989)].

Such tetrahedral edge rotation, of necessity, leads to a shrinkage in cell dimensions (dependent upon the magnitude of the angle of rotation) in the plane perpendicular to the $\langle 110 \rangle$ tetrahedral edge around which such rotation takes place (see Figs. 3 and 4). In the case of low carnegieite, the resultant space-group symmetry and unit-cell dimensions (the relationship between the cell dimensions of the C9 aristotype and the resultant low carnegieite structure are shown in Fig. 5) are only compatible with tetrahedral edge rotation around the mutually orthogonal $(\mathbf{a} + \mathbf{c})_{C9} = \mathbf{a}'$ and $(-\mathbf{a} + \mathbf{c})_{C9} = \mathbf{c}'$ axes. (Tetrahedral rotation around the $2\mathbf{b}_{C9} = \mathbf{b}'$ axis is incompatible with the resultant space-group symmetry).

Indeed, given the cubic aristotype unit-cell dimension of 7.808 Å, the observed cell parameters of low carnegieite require that the magnitude of tetrahedral rotation of all the framework tetrahedra about both the resultant $\mathbf{c}'$ axis, θ_z, as well as about the resultant $\mathbf{a}'$ axis, θ_x, must both be of the order of $\sim 20°$. Assuming an averaged (Al,Si)O$_4$ tetrahedron, it is not difficult to show (see Figs. 3 and 4) that:

$$a' = 7.808 \times 2^{1/2}\cos(\theta_z),$$

$$b' = 2 \times 7.808/(1 + \tan^2\theta_x + \tan^2\theta_z)^{1/2}$$

and $c' = (7.808 \times 2^{1/2}/2)\cos(\theta_x).$

For rotation angles $\theta_x = 19.4$ and $\theta_z = 20.2°$, the predicted resultant cell parameters would be 10.363, 13.915 and 5.208 Å, all within 1% of their experimentally determined values. It is clear, therefore, that by far the major component of the structural deviation of the low carnegieite structure from its underlying C9 aristotype arises from coupled tetrahedral edge rotations of magnitude $\sim 20°$ about the mutually orthogonal $(\mathbf{a} + \mathbf{c})_{C9} = \mathbf{a}'$ and the $(-\mathbf{a} + \mathbf{c})_{C9} = \mathbf{c}'$ axes. In order to derive a plausible starting model for subsequent Rietveld refinement we therefore need only ascribe non-zero values to those structural degrees of freedom associated with such tetrahedral edge rotation.

2.3. Defining the modulation functions

Formally the deviation of the resultant structure from the above average structure must be able to be expressed in terms of compositional and displacive modulations as follows (see, for example, Perez-Mato et al., 1987; Yamamoto, 1982):

$$\delta f_\mu(\mathbf{T}) = f_\mu^{av}\mathrm{Re}\{\sum_\mathbf{q} a_\mu(\mathbf{q})\cos[2\pi\mathbf{q}.\mathbf{T} + \theta_\mu(\mathbf{q})]\} \quad (1)$$

$$\mathbf{u}_\mu(\mathbf{T}) = \mathrm{Re}\{\sum_\mathbf{q} \sum_{\alpha=a,b,c} \alpha\varepsilon_{\mu\alpha}(\mathbf{q})\cos[2\pi\mathbf{q}.\mathbf{T} + \theta_{\mu\alpha}(\mathbf{q})]\}. \quad (2)$$

Here $\delta f_\mu(\mathbf{T})$ represents the deviation (from f_μ^{av}) of the atomic scattering factor of the μth atom in the Tth parent primitive unit cell, while $\mathbf{u}_\mu(\mathbf{T})$ represents the atomic displacement away from its position in the parent structure $(\mathbf{r}_\mu + \mathbf{T})$ of the μth atom in the Tth parent primitive unit cell. The compositional component of a modulation characterized by the modulation wavevector $\mathbf{q}$ is specified by its compositional eigenvector components $A_\mu(\mathbf{q}) = a_\mu(\mathbf{q})\exp[i\theta_\mu(\mathbf{q})]$ while the displacive component is specified by its displacement eigenvector components

Fig. 4. The effect of tetrahedral edge rotation around the $2\mathbf{c}' = (-\mathbf{a} + \mathbf{c})_{C9}$ direction. Such tetrahedral edge rotation must lead to a shrinkage of the resultant unit-cell dimensions along both the $\mathbf{a}'$ and $\mathbf{b}'$ directions. Similar tetrahedral edge rotation around the orthogonal $\mathbf{a}' = (\mathbf{a} + \mathbf{c})_{C9}$ direction leads to a shrinkage of the resultant unit-cell dimensions along the $\mathbf{c}'$ and $\mathbf{b}'$ directions.
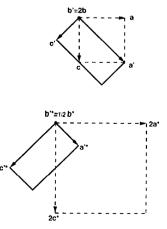

Fig. 5. The real and reciprocal space unit-cell relationships between the aristotype (unprimed) and the resultant low carnegieite structure (primed).

$e_{\mu\alpha}(\mathbf{q}) = \varepsilon_{\mu\alpha}(\mathbf{q})\exp[i\theta_{\mu\alpha}(\mathbf{q})]$ where the $e_{\mu\alpha}$'s represent the shifts of the μth atom along the αth (= $\mathbf{a}$, $\mathbf{b}$ or $\mathbf{c}$) direction of the underlying average structure. If such modulations have non-zero amplitude, they will give rise to satellite reflections at $\mathbf{G}_p \pm \mathbf{q}$, where $\mathbf{G}_p$ is a Bravais lattice allowed reflection of the average structure.

Such modulations are characterized by their transformation properties under the space-group symmetry operations belonging to the little group of the corresponding modulation wavevector. It is often the case that compositional and/or displacement modulations associated with specific modulation wavevectors transform according to a particular irreducible representation of the corresponding little co-group (see, for example, Withers, Hua, Welberry & Vincent, 1988). Consequently such modulations often give rise to characteristic satellite extinction conditions. The observation of such characteristic extinction conditions (for example the systematic absences observed at the [100] and [001] zone axes of low carnegieite as a result of the b and a glides perpendicular to the $\mathbf{a}'$ and $\mathbf{c}'$ axes respectively, see Fig. 2) can then be used to eliminate potential degrees of freedom and to derive the most general possible atomic displacement pattern associated with each modulation wavevector.

2.4. Independent modulation wavevectors

The real and reciprocal space unit-cell relationships between the C9-related reference structure and the $Pb2_1a$ resultant structure are shown in Fig. 5. The additional satellite reflections which accompany the strong matrix reflections of the parent structure in the case of low carnegieite are characterized by the modulation wavevectors $\mathbf{q}_1 = \frac{1}{4}(020)^*$, $\mathbf{q}_2 = \frac{1}{4}(202)^*$, $\mathbf{q}_3 = \frac{1}{4}(222)^*$, $\mathbf{q}_4 = \frac{1}{4}(\bar{2}2\bar{2})^*$, $\mathbf{q}_5 = (010)^*$ and $\mathbf{q}_6 = 0$. The determination of the structure of low carnegieite is equivalent to the determination of the compositional and displacement eigenvector components associated with each of these independent modulation wavevectors.

2.5. Irreducible representations and eigenvectors associated with the various modulation wavevectors

The little co-groups $\mathbf{G}^q$ corresponding to the various symmetry points and lines of the first Brillouin zone of the primitive Γ_c^f Bravais lattice appropriate to the $Fd3m$ C9 aristotype have been tabulated and can be looked up in, for example, Bradley & Cracknell (1972). The subgroups of these little co-groups whose elements belong to mmm correspond to the little co-groups appropriate to the strain-deformed C9-type reference structure.

2.5.1. The $\mathbf{q}_1 = \frac{1}{4}(020)^*$ modulation. The corresponding little co-group $\mathbf{G}^{q_1}$ of this modulation wavevector is that subgroup of $mmm = \{E, C_{2c}, C_{2e}, C_{2y}, i, \sigma_{dc}, \sigma_{de}, \sigma_y\}$ which leaves $\mathbf{q}$ invariant modulo an allowed matrix reflection, namely $\mathbf{G}^{q_1} = \{E, C_{2y}, \sigma_{dc}, \sigma_{de}\}$ where the symmetry operations are defined in Fig. 1.3 of

Table 1. *Multiplication table corresponding to the little co-group of* $\mathbf{q}_1$

	E	C_{2y}	σ_{dc}	σ_{de}
R_1	1	1	1	1
R_2	1	1	-1	-1
R_3	1	-1	1	-1
R_4	1	-1	-1	1

Bradley & Cracknell (1972) and also in Fig. 3. Note that the symmetry operation σ_{dc} corresponds to reflection in a plane perpendicular to the resultant $\mathbf{a}'$ axis whereas the symmetry operation σ_{de} corresponds to reflection in a plane perpendicular to the resultant $\mathbf{c}'$ axis. The multiplication table corresponding to this little co-group is given in Table 1. There are four one-dimensional irreducible representations labelled R_1 to R_4. Only an R_4 irreducible representation, however, is compatible with the resultant space-group symmetry of $Pb2_1a$.

Note that a character of -1 under σ_{dc}, for example, implies that the atomic displacement pattern associated with $\mathbf{q}_1$ maps into the negative of itself under the symmetry operation σ_{dc}. As $2\pi\mathbf{q}_1.[\frac{1}{2}(\mathbf{a} + \mathbf{c}) + \mathbf{b}] = \pi$, it therefore follows that the atomic displacement pattern associated with $\mathbf{q}_1$ maps into itself under $\{\sigma_{dc}|\frac{1}{2}(\mathbf{a} + \mathbf{c}) + \mathbf{b}\}$ as required by the resultant space-group symmetry. Note that $\{\sigma_{dc}|\frac{1}{2}(\mathbf{a} + \mathbf{c}) + \mathbf{b}\}$ is equivalent to $\{\sigma_x|\frac{1}{2}(\mathbf{a}' + \mathbf{b}')\}$ (*i.e.* the b glide perpendicular to $\mathbf{a}'$) in terms of the resultant structure. Similarly a character of $+1$ under σ_{de} implies that the atomic displacement pattern associated with $\mathbf{q}_1$ maps into itself under $\{\sigma_{de}|\frac{1}{2}(\mathbf{a} + \mathbf{c})\}$ as also required by the resultant space-group symmetry, *i.e.* $\{\sigma_{de}|\frac{1}{2}(\mathbf{a} + \mathbf{c})\}$ is equivalent to $\{\sigma_z|\frac{1}{2}\mathbf{a}'\}$ (the a glide perpendicular to $\mathbf{c}'$) in terms of the resultant structure.

Application of standard group theoretical techniques (see, for example, Withers, Wallenberg, Bevan, Thompson & Hyde, 1989) shows that compositional modulation of the metal-atom occupancies is not allowed for this modulation wavevector and gives the most general possible atomic displacement pattern associated with the modulation wavevector $\mathbf{q}_1$ as:

$$\mathbf{u}_{M1}(\mathbf{T}) = 2^{1/2}\varepsilon_{M1}(\mathbf{q}_1)\cos[2\pi\mathbf{q}_1.\mathbf{T} + \varphi_{M1}(\mathbf{q}_1)](\mathbf{a} + \mathbf{c})$$

$$\mathbf{u}_{M2}(\mathbf{T}) = 2^{1/2}\varepsilon_{M2}(\mathbf{q}_1)\cos[2\pi\mathbf{q}_1.\mathbf{T} + \varphi_{M2}(\mathbf{q}_1)](\mathbf{a} + \mathbf{c})$$

$$\mathbf{u}_{Na1}(\mathbf{T}) = \varepsilon_{Na1}(\mathbf{q}_1)\cos[2\pi\mathbf{q}_1.\mathbf{T} + \varphi_{Na1}(\mathbf{q}_1)](\mathbf{a} + \mathbf{c})$$

$$\mathbf{u}_{Na2}(\mathbf{T}) = \varepsilon_{Na2}(\mathbf{q}_1)\cos[2\pi\mathbf{q}_1.\mathbf{T} + \varphi_{Na2}(\mathbf{q}_1)](\mathbf{a} + \mathbf{c})$$

$$\mathbf{u}_{O1}(\mathbf{T}) = 2^{1/2}\varepsilon_{O1}(\mathbf{q}_1)\cos[2\pi\mathbf{q}_1.\mathbf{T} + \varphi_{O1}(\mathbf{q}_1)](\mathbf{a} + \mathbf{c})$$
$$- 2^{1/2}\varepsilon_{O1}{}^y(\mathbf{q}_1)\cos[2\pi\mathbf{q}_1.\mathbf{T} + \varphi_{O1}{}^y(\mathbf{q}_1)]\mathbf{b}$$

$$\mathbf{u}_{O3}(\mathbf{T}) = 2^{1/2}\varepsilon_{O1}(\mathbf{q}_1)\cos[2\pi\mathbf{q}_1.\mathbf{T} + \varphi_{O1}(\mathbf{q}_1)](\mathbf{a} + \mathbf{c})$$
$$+ 2^{1/2}\varepsilon_{O1}{}^y(\mathbf{q}_1)\cos[2\pi\mathbf{q}_1.\mathbf{T} + \varphi_{O1}{}^y(\mathbf{q}_1)]\mathbf{b}$$

$$\mathbf{u}_{O2}(\mathbf{T}) = \varepsilon_{O2}(\mathbf{q}_1)\cos[2\pi\mathbf{q}_1.\mathbf{T} + 45° + \varphi_{O2}(\mathbf{q}_1)](\mathbf{a} + \mathbf{c})$$
$$= \mathbf{u}_{O4}(\mathbf{T}).$$

Thus, formally there are 14 independent displacive degrees of freedom associated with just this q_1 modulation wavevector, ten of which are associated with the framework tetrahedra. If, however, we make the reasonable assumption that by far the major component of the structural deviation of low carnegieite from the average structure will be as a result of tetrahedral edge rotation of the framework tetrahedra, then this number of free parameters can be reduced significantly. The above atomic displacement pattern is not compatible with tetrahedral edge rotation around the $(a + c)_{C9} = a'$ axes but is compatible with tetrahedral edge rotation around the $(-a + c)_{C9} = c'$ axes.

The assumption of tetrahedral regularity in conjunction with the requirement that each tetrahedra should rotate through an angle of the same magnitude requires that $\varphi_{M1}(q_1) = \varphi_{M2}(q_1) = 45°$, $\varphi_{O1}{}^y(q_1) = \varphi_{O1}(q_1) = 45°$, $\varepsilon_{M1}(q_1) = \varepsilon_{M2}(q_1) = \varepsilon_{Mx}(q_1)$, $\varepsilon_{O2}(q_1) = 0$ and that $\varepsilon_{O1}{}^y(q_1) = \varepsilon_{O1}(q_1) = 2\varepsilon_{Mx}(q_1)$ (see Fig. 6). Thus the ten degrees of freedom associated with framework tetrahedral rotation can be reduced to just one, namely $\varepsilon_{Mx}(q_1)$. Furthermore a rotation angle of 20.2° around the c' axis and 19.4° around the a' axes requires a value for $\varepsilon_{Mx}(q_1)$ in the close vicinity of 0.033.

2.5.2. The $q_2 = \frac{1}{4}(202)*$ modulation. The corresponding little co-group G^{q_2} of this modulation wavevector is that subgroup of mmm which leaves q invariant modulo an allowed matrix reflection, namely $G^{q_2} = \{E, \sigma_{de}\}$. There are only two one-dimensional irreducible representations labelled R_1 (the totally symmetric representation) and R_2. Only an R_2 irreducible representation, however, is compatible with the resultant space-group symmetry of $Pb2_1a$. A character of -1 under σ_{de}, as required by an R_2 irreducible representation, implies that the atomic displacement pattern associated with q_2 maps into itself under $\{\sigma_{de}|\frac{1}{2}(a + c)\}$ as also required by the resultant space-group symmetry i.e. $\{\sigma_{de}|\frac{1}{2}(a + c)\}$ is equivalent to $\{\sigma_z|\frac{1}{2}a'\}$ (the a glide perpendicular to c') in terms of the resultant structure.
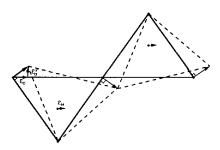

Fig. 6. The relationship between the C9-related average (i.e. with the effects of strain in the unit-cell parameters already incorporated) structure (in bold) and the tetrahedral edge rotated structure (dashed lines). The assumption of tetrahedral regularity in conjunction with the requirement that each tetrahedra should rotate through the same angle requires that $\varepsilon_O{}^y = \varepsilon_O = 2\varepsilon_M$.

Similar considerations to the above for this $q_2 = \frac{1}{4}(202)*$ modulation wavevector show that compositional modulation of the metal-atom occupancies is again not allowed and that the most general possible atomic displacement pattern compatible with the resultant space-group symmetry of $Pb2_1a$ is given by:

$$u_{M1}(T) = \varepsilon_{M1}(q_2)\cos(2\pi q_2.T + 90°)(-a + c)$$

$$u_{M2}(T) = -\varepsilon_{M2}(q_2)\cos(2\pi q_2.T + 0°)(-a + c)$$

$$u_{Na1}(T) = \varepsilon_{Na1}(q_2)\cos(2\pi q_2.T + 90°)(-a + c)$$

$$u_{Na2}(T) = \varepsilon_{Na2}(q_2)\cos(2\pi q_2.T + 0°)(-a + c)$$

$$u_{O1}(T) = \varepsilon_{O1}(q_2)\cos(2\pi q_2.T + 90°)(-a + c)$$

$$u_{O3}(T) = -\varepsilon_{O1}(q_2)\cos(2\pi q_2.T + 90°)(-a + c)$$

$$u_{O2}(T) = \varepsilon_{O2}{}^x(q_2)\cos[2\pi q_2.T + \varphi_{O2}{}^x(q_2)](a + c)$$
$$- \varepsilon_{O2}{}^y(q_2)\cos(2\pi q_2.T + 90°)b$$
$$+ \varepsilon_{O2}{}^z(q_2)\cos(2\pi q_2.T + 90°)(-a + c)$$

$$u_{O4}(T) = -\varepsilon_{O2}{}^x(q_2)\cos[2\pi q_2.T + \varphi_{O2}{}^x(q_2)](a + c)$$
$$+ \varepsilon_{O2}{}^y(q_2)\cos(2\pi q_2.T + 90°)b$$
$$+ \varepsilon_{O2}{}^z(q_2)\cos(2\pi q_2.T + 90°)(-a + c).$$

This time the atomic displacement pattern is only compatible with tetrahedral edge rotation around the $(a + c)_{C9} = a'$ axes. Unlike the situation for the q_1 displacive modulation, however, the resultant space-group symmetry (specifically the requirement that the resultant structure should have a b glide perpendicular to a', i.e. that $\{\sigma_{dc}|\frac{1}{2}(a + c) + b\}$ must be a symmetry operation of the resultant structure) fixes most of the phase angles in the associated atomic displacement pattern associated with the q_2 displacive modulation. In particular, the resultant space-group symmetry requires that only alternate sheets of tetrahedra (perpendicular to a') rotate around a' as far as the atomic displacement pattern associated with this q_2 displacive modulation is concerned, i.e. $u_M(T = 0a' + \ldots) = u_M(T = \frac{1}{2}a' + \ldots)$ $= 0$. (It will be shown below that the requirement that each tetrahedra should rotate through the same angle in the overall resultant structure can still be met because the q_3 and q_4 displacive modulations are intimately linked and combine in such a way as to rotate the tetrahedral sheets not rotated by this q_2 modulation.)

The assumption of tetrahedral regularity implies that $\varepsilon_{M1}(q_2) = \varepsilon_{M2}(q_2) = \varepsilon_{Mz}(q_2)$, $\varepsilon_{O1}(q_2) = 0 = \varepsilon_{O2}{}^x(q_2)$ and that $\varepsilon_{O2}{}^y(q_2) = \varepsilon_{O2}{}^z(q_2) = 2\varepsilon_{Mz}(q_2)$ (see Fig. 6). Thus the seven degrees of freedom associated with framework tetrahedral rotation are again reduced to just one, namely $\varepsilon_{Mz}(q_2)$. A rotation angle of 20.2° around the c' axis and 19.4° around the a' axes requires a value for $\varepsilon_{Mz}(q_2)$ in the close vicinity of 0.031.

2.5.3. The $q_3 = \frac{1}{4}(222)^*$ and $q_4 = \frac{1}{4}(\bar{2}2\bar{2})^*$ modulations. Symmetry elements of the resultant space-group symmetry (specifically the b glide perpendicular to a') link these two modulation wavevectors and hence their eigenvectors are intimately related. The corresponding little co-groups G^{q_3} and G^{q_4} of these modulation wavevectors is that subgroup of mmm which leaves q_3 and q_4 invariant modulo an allowed matrix reflection, namely $G^{q_3} = G^{q_4} = \{E, \sigma_{de}\}$, the same as for q_2 above. Again only the R_2 irreducible representation is compatible with the resultant space-group symmetry of $Pb2_1a$, i.e. a character of -1 under σ_{de} implies that the atomic displacement pattern associated with q_3 and q_4 maps into itself under $\{\sigma_{de}|\frac{1}{2}(a + c)\}$ as also required by the resultant space-group symmetry, i.e. $\{\sigma_{de}|\frac{1}{2}(a + c)\}$ is equivalent to $\{\sigma_z|\frac{1}{2}a'\}$ (the a glide perpendicular to c') in terms of the resultant structure.

Again compositional modulation of the metal-atom occupancies is not allowed while the most general possible atomic displacement pattern associated with the q_3 and q_4 modulation wavevectors and compatible with the resultant $Pb2_1a$ space-group symmetry is given by:

$$u_{M1}(T) = \tfrac{1}{2}\varepsilon_{M1}(q_3,q_4)(\cos 2\pi q_3.T$$
$$+ \cos 2\pi q_4.T)(-a + c)$$

$$u_{M2}(T) = \tfrac{1}{2}\varepsilon_{M2}(q_3,q_4)(-\cos 2\pi q_3.T$$
$$+ \cos 2\pi q_4.T)(-a + c)$$

$$u_{Na1}(T) = \tfrac{1}{2}\varepsilon_{Na1}(q_3,q_4)(\cos 2\pi q_3.T$$
$$+ \cos 2\pi q_4.T)(-a + c)$$

$$u_{Na2}(T) = \tfrac{1}{2}\varepsilon_{Na2}(q_3,q_4)(-\cos 2\pi q_3.T$$
$$+ \cos 2\pi q_4.T)(-a + c)$$

$$u_{O1}(T) = [\varepsilon_{O1}{}^+(q_3,q_4)\cos 2\pi q_3.T$$
$$+ \varepsilon_{O1}{}^-(q_3,q_4)\cos 2\pi q_4.T](-a + c)$$

$$u_{O3}(T) = [\varepsilon_{O1}{}^-(q_3,q_4)\cos 2\pi q_3.T$$
$$+ \varepsilon_{O1}{}^+(q_3,q_4)\cos 2\pi q_3.T](-a + c)$$

$$u_{O2}(T) = \tfrac{1}{2}\varepsilon_{O2}{}^x(q_3,q_4)[\cos 2\pi q_3.T$$
$$- \cos 2\pi q_4.T](a + c) + [\cos 2\pi q_3.T$$
$$+ \cos 2\pi q_4.T][-\tfrac{1}{2}\varepsilon_{O2}{}^y(q_3,q_4)b$$
$$+ \tfrac{1}{2}\varepsilon_{O2}{}^z(q_3,q_4)(-a + c)]$$

$$u_{O4}(T) = -\tfrac{1}{2}\varepsilon_{O2}{}^x(q_3,q_4)[\cos 2\pi q_3.T$$
$$- \cos 2\pi q_4.T](a + c) + [\cos 2\pi q_3.T$$
$$+ \cos 2\pi q_4.T][\tfrac{1}{2}\varepsilon_{O2}{}^y(q_3,q_4)b$$
$$+ \tfrac{1}{2}\varepsilon_{O2}{}^z(q_3,q_4)(-a + c)].$$

This atomic displacement pattern is not compatible with tetrahedral rotation around the $(-a + c)_{C9} = c'$ axes but is compatible with tetrahedral rotation around the $(a + c)_{C9} = a'$ axes. As for the q_2 modulation, the resultant space-group symmetry requires that only alternate sheets of tetrahedra (perpendicular to a') rotate around a' but this time the tetrahedral sheets which rotate are precisely the ones which did not rotate in the case of the q_2 modulation. The assumption of tetrahedral regularity requires that $\varepsilon_{M1}(q_3,q_4) = \varepsilon_{M2}(q_3,q_4) = \varepsilon_{Mz}(q_3,q_4)$, $\varepsilon_{O1}{}^+(q_3,q_4) = \varepsilon_{O1}{}^-(q_3,q_4) = 0$, $\varepsilon_{O2}{}^x(q_3,q_4) = 0$ and that $\varepsilon_{O2}{}^y(q_3,q_4) = \varepsilon_{O2}{}^z(q_3,q_4) = 2\varepsilon_{Mz}(q_3,q_4)$. Thus the seven degrees of freedom associated with framework tetrahedral rotation are again reduced to just one, namely $\varepsilon_{Mz}(q_3,q_4)$. Furthermore the assumption that the magnitude of the angle each tetrahedron rotates through should be the same requires that the magnitude of $\varepsilon_{Mz}(q_3,q_4)$ must equal the magnitude of $\varepsilon_{Mz}(q_2)$. A rotation angle of $19.4°$ around both the a' axis requires a value for this magnitude in the close vicinity of 0.031. The remaining degree of freedom as far as tetrahedral rotation around the a' axis is concerned is the relative sign of $\varepsilon_{Mz}(q_3,q_4)$ and $\varepsilon_{Mz}(q_2)$. This sign choice will be shown below to lead to two distinct plausible starting models for the Rietveld refinement.

2.5.4. The $q_5 = (010)^*$ modulation. Compositional modulation of the metal-atom occupancies is allowed for this modulation wavevector. The most general possible occupancy modulation function associated with this q_5 modulation wavevector and compatible with the resultant $Pb2_1a$ space-group symmetry is given by:

$$f_{M1}(T) = \tfrac{1}{2}(f_{Al} + f_{Si})\{1 + a_{M1}(q_5)\cos[2\pi q_5.T$$
$$+ \theta_{M1}(q_5)]\}$$

$$f_{M2}(T) = \tfrac{1}{2}(f_{Al} + f_{Si})\{1 + a_{M2}(q_5)\cos[2\pi q_5.T$$
$$+ \theta_{M2}(q_5)]\}$$

$$f_{Na1}(T) = \tfrac{1}{2}(f_{Na})\{1 + a_{Na1}(q_5)\cos[2\pi q_5.T + \theta_{Na1}(q_5)]\}$$

$$f_{Na2}(T) = \tfrac{1}{2}(f_{Na})\{1 + a_{Na2}(q_5)\cos[2\pi q_5.T + \theta_{Na2}(q_5)]\}.$$

Fourier decomposition of the recently reported crystal structure of $Na_{1-x}[Fe_{1-x}Si_xO_2]$, $0.10 < x < 0.25$ (Grey et al., 1990), in the above terms shows that just such a $q_5 = b^*$ compositional modulation occurs in this system and leads to planes of tetrahedra perpendicular to our a' being alternately Fe-rich and Si-rich. In the case of low carnegieite, solid-state NMR evidence requires each SiO_4 tetrahedra to be surrounded by four AlO_4 tetrahedra and vice versa (Thompson et al., 1993). Such tetrahedral cation ordering cannot be described by a q_5 compositional modulation and indeed requires that $a_{M1}(q_5) = a_{M2}(q_5) = 0$. It cannot necessarily be assumed, however, that $a_{Na1}(q_5)$ and $a_{Na2}(q_5)$ are zero for low carnegieite.

The most general possible atomic displacement pattern associated with the q_5 modulation wavevector and compatible with the resultant $Pb2_1a$ space-group symmetry is given by:

$$\mathbf{u}_{M1}(T) = \varepsilon_{M1}(q_5)(\cos 2\pi q_5.T)\mathbf{b}$$

$$\mathbf{u}_{M2}(T) = \varepsilon_{M2}(q_5)(\cos 2\pi q_5.T)\mathbf{b}$$

$$\mathbf{u}_{Na1}(T) = \varepsilon_{Na1}(q_5)(\cos 2\pi q_5.T)\mathbf{b}$$

$$\mathbf{u}_{Na2}(T) = \varepsilon_{Na2}(q_5)(\cos 2\pi q_5.T)\mathbf{b}$$

$$\mathbf{u}_{O1}(T) = [\varepsilon_{O1}(q_5)(\mathbf{a} + \mathbf{c}) + \varepsilon_{O1}{}^y(q_5)\mathbf{b}](\cos 2\pi q_5.T)$$

$$\mathbf{u}_{O3}(T) = [-\varepsilon_{O1}(q_5)(\mathbf{a} + \mathbf{c}) + \varepsilon_{O1}{}^y(q_5)\mathbf{b}](\cos 2\pi q_5.T)$$

$$\mathbf{u}_{O2}(T) = [\varepsilon_{O2}{}^y(q_5)\mathbf{b} + \varepsilon_{O2}{}^z(q_5)(-\mathbf{a} + \mathbf{c})](\cos 2\pi q_5.T)$$

$$\mathbf{u}_{O4}(T) = [\varepsilon_{O2}{}^y(q_5)\mathbf{b} - \varepsilon_{O2}{}^z(q_5)(-\mathbf{a} + \mathbf{c})](\cos 2\pi q_5.T).$$

The above atomic displacement pattern is not compatible with tetrahedral edge rotation around either the $\mathbf{a}'$ or $\mathbf{c}'$ axes and hence for the purposes of deriving a plausible starting model all of the above degrees of freedom associated with the tetrahedral framework can be assumed to be zero.

2.5.5. The $q_6 = 0$ modulation. Compositional modulation of the metal-atom occupancies is also allowed for this modulation wavevector. The most general possible occupancy modulation function associated with this $q_6 = 0$ modulation wavevector and compatible with the resultant $Pb2_1a$ space-group symmetry is this time given by:

$$f_{M1}(T) = \tfrac{1}{2}(f_{Al} + f_{Si})[1 + a_{M1}(q_6)]$$

$$f_{M2}(T) = \tfrac{1}{2}(f_{Al} + f_{Si})[1 + a_{M2}(q_6)]$$

$$f_{Na1}(T) = \tfrac{1}{2}(f_{Na})[1 + a_{Na1}(q_6)]$$

$$f_{Na2}(T) = \tfrac{1}{2}(f_{Na})[1 + a_{Na2}(q_6)].$$

The solid-state NMR requirement that each SiO_4 tetrahedra is surrounded by four AlO_4 tetrahedra and vice versa is equivalent to requiring that $\tfrac{1}{2}(f_{Al} + f_{Si})a_{M2}(q_6) = -\tfrac{1}{2}(f_{Al} + f_{Si})a_{M1}(q_6) = -\tfrac{1}{2}(f_{Al} - f_{Si})$. Note that $a_{Na1}(q_6) = a_{Na2}(q_6) = 0$ implies half occupancy of Na1 and Na2 sites whereas $\tfrac{1}{2}(f_{Na})a_{Na2}(q_6) = -\tfrac{1}{2}(f_{Na})a_{Na1}(q_6) = +1$ or -1 implies full occupancy of either the Na1 or Na2 sites, respectively, as can be seen by substitution into the above occupancy modulation function.

Finally, the most general possible atomic displacement pattern associated with this q_6 modulation wavevector and compatible with the $Pb2_1a$ resultant space-group symmetry is given by:

$$\mathbf{u}_{M1}(T) = \varepsilon_{M1}(q_6)\mathbf{b}$$

$$\mathbf{u}_{M2}(T) = \varepsilon_{M2}(q_6)\mathbf{b}$$

$$\mathbf{u}_{Na1}(T) = \varepsilon_{Na1}(q_6)\mathbf{b}$$

$$\mathbf{u}_{Na2}(T) = \varepsilon_{Na2}(q_6)\mathbf{b}$$

$$\mathbf{u}_{O1}(T) = \varepsilon_{O1}{}^x(q_6)(\mathbf{a} + \mathbf{c}) + \varepsilon_{O1}{}^y(q_6)\mathbf{b}$$

$$\mathbf{u}_{O3}(T) = -\varepsilon_{O1}{}^x(q_6)(\mathbf{a} + \mathbf{c}) + \varepsilon_{O1}{}^y(q_6)\mathbf{b}$$

$$\mathbf{u}_{O2}(T) = -\varepsilon_{O2}{}^z(q_6)(-\mathbf{a} + \mathbf{c}) - \varepsilon_{O2}{}^y(q_6)\mathbf{b}$$

$$\mathbf{u}_{O4}(T) = + \varepsilon_{O2}{}^z(q_6)(-\mathbf{a} + \mathbf{c}) - \varepsilon_{O2}{}^y(q_6)\mathbf{b}.$$
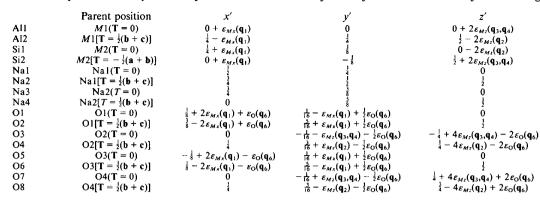
Again the above atomic displacement pattern is not compatible with tetrahedral edge rotation around either the $\mathbf{a}'$ or $\mathbf{c}'$ axes and hence $\varepsilon_{M1}(q_6)$ and $\varepsilon_{M2}(q_6)$ can be put to zero. The shifts of the framework O atoms, however, are required to be non-zero in order to take account of the slightly different size of the SiO_4 and AlO_4 tetrahedra relative to the average tetrahedral size. The assumption of tetrahedral regularity requires that $\varepsilon_{O1}{}^x(q_6) = \varepsilon_{O1}{}^y(q_6) = \varepsilon_{O2}{}^z(q_6) = \varepsilon_{O2}{}^y(q_6) = \varepsilon_O(q_6) \simeq 0.006$.

Determination of the 48 displacive and eight compositional degrees of freedom associated with the above modulation functions is equivalent to determination of the structure of low carnegieite. In order to derive a plausible starting model for Rietveld refinement, however, only those degrees of freedom associated with tetrahedral edge rotation and with the Al/Si ordering need be considered. Taking only these degrees of freedom into account and re-expressing the above modulation functions in terms of the resultant unit cell, gives the fractional coordinates listed in Table 2.

It is interesting to note that the $q_6 = 0$ mode is the only one to destroy the symmetry operation $\{\sigma_y|\tfrac{1}{4}(-\mathbf{a} -\mathbf{b} + \mathbf{c})\}_{C9}$ (equivalent to $\{\sigma_y|(-\tfrac{1}{8}\mathbf{b}' + \tfrac{1}{2}\mathbf{c}')\}$ in terms of the resultant structure) and hence lower the resultant space-group symmetry from $Pbca$ to the observed $Pb2_1a$. [The absence of such a mode in the case of $KGaO_2$ and $Na_{1-x}[Fe_{1-x}Si_xO_2]$, $0.10 < x < 0.25$ (Grey et al., 1990), is thus consistent with the higher space-group symmetries reported for these materials.] Application of this operation to the resultant structure is thus equivalent to flipping the sign of this $q_6 = 0$ mode.

In order that each tetrahedra rotates through an angle of the same magnitude around the $\mathbf{a}'$ axis, $|\varepsilon_{Mz}(q_3,q_4)| = |\varepsilon_{Mz}(q_2)|$. Furthermore, in order that each tetrahedra remains as close to regular as possible, $|\varepsilon_{Mz}(q_3,q_4)| = |\varepsilon_{Mz}(q_2)| \simeq 0.0312$, $|\varepsilon_{Mx}(q_1)| \simeq 0.0327$ and $\varepsilon_O(q_6) \simeq 0.0056$. For example, choosing $\tfrac{1}{2}(f_{Al} + f_{Si})a_{M2}(q_6) = -\tfrac{1}{2}(f_{Al} + f_{Si})a_{M1}(q_6) = -\tfrac{1}{2}(f_{Al} - f_{Si})$, $\varepsilon_{Mx}(q_1) = -0.0312$, $\varepsilon_{Mz}(q_2) = -0.0312$, $\varepsilon_{Mz}(q_3,q_4) = +0.0312$ and $\varepsilon_O(q_6) = 0.0056$ results in Al—O distances within AlO_4 tetrahedra of 1.750 ± 0.018 Å, Si—O distances within SiO_4 tetrahedra of 1.621 ± 0.013 Å, O—O distances within AlO_4 tetrahedra of 2.843 ± 0.032 Å and O—O distances within SiO_4 tetrahedra of 2.660 ± 0.079 Å. The ideal corresponding values would be 1.757, 1.624, 2.869 and 2.652 Å, respectively. While not completely exact the

Table 2. *Group theoretically derived fractional coordinates for the framework atoms of low carnegeite*

	Parent position	x'	y'	z'
Al1	$M1(T = 0)$	$0 + \varepsilon_{Mx}(q_1)$	0	$0 + 2\varepsilon_{Mz}(q_3,q_4)$
Al2	$M1[T = \frac{1}{2}(b + c)]$	$\frac{1}{4} - \varepsilon_{Mx}(q_1)$	$\frac{1}{4}$	$\frac{1}{2} - 2\varepsilon_{Mz}(q_2)$
Si1	$M2(T = 0)$	$\frac{1}{4} + \varepsilon_{Mx}(q_1)$	$\frac{1}{4}$	$0 - 2\varepsilon_{Mz}(q_2)$
Si2	$M2[T = -\frac{1}{2}(a + b)]$	$0 + \varepsilon_{Mx}(q_1)$	$-\frac{1}{8}$	$\frac{1}{2} + 2\varepsilon_{Mz}(q_3,q_4)$
Na1	$Na1(T = 0)$	$\frac{1}{2}$	$\frac{1}{4}$	0
Na2	$Na1[T = \frac{1}{2}(b + c)]$	$\frac{3}{4}$	$\frac{1}{2}$	$\frac{1}{2}$
Na3	$Na2(T = 0)$	$\frac{3}{4}$	$\frac{3}{8}$	0
Na4	$Na2[T = \frac{1}{2}(b + c)]$	0	$\frac{5}{8}$	$\frac{1}{2}$
O1	$O1(T = 0)$	$\frac{1}{8} + 2\varepsilon_{Mx}(q_1) + \varepsilon_O(q_6)$	$\frac{1}{16} - \varepsilon_{Mx}(q_1) + \frac{1}{2}\varepsilon_O(q_6)$	0
O2	$O1[T = \frac{1}{2}(b + c)]$	$\frac{3}{8} - 2\varepsilon_{Mx}(q_1) + \varepsilon_O(q_6)$	$\frac{5}{16} + \varepsilon_{Mx}(q_1) + \frac{1}{2}\varepsilon_O(q_6)$	$\frac{1}{2}$
O3	$O2(T = 0)$	0	$-\frac{1}{16} - \varepsilon_{Mz}(q_3,q_4) - \frac{1}{2}\varepsilon_O(q_6)$	$-\frac{1}{4} + 4\varepsilon_{Mz}(q_3,q_4) - 2\varepsilon_O(q_6)$
O4	$O2[T = \frac{1}{2}(b + c)]$	$\frac{1}{4}$	$\frac{3}{16} + \varepsilon_{Mz}(q_2) - \frac{1}{2}\varepsilon_O(q_6)$	$\frac{1}{4} - 4\varepsilon_{Mz}(q_2) - 2\varepsilon_O(q_6)$
O5	$O3(T = 0)$	$-\frac{1}{8} + 2\varepsilon_{Mx}(q_1) - \varepsilon_O(q_6)$	$\frac{1}{16} + \varepsilon_{Mx}(q_1) + \frac{1}{2}\varepsilon_O(q_6)$	0
O6	$O3[T = \frac{1}{2}(b + c)]$	$\frac{3}{8} - 2\varepsilon_{Mx}(q_1) - \varepsilon_O(q_6)$	$\frac{5}{16} - \varepsilon_{Mx}(q_1) + \frac{1}{2}\varepsilon_O(q_6)$	$\frac{1}{2}$
O7	$O4(T = 0)$	0	$-\frac{1}{16} + \varepsilon_{Mz}(q_3,q_4) - \frac{1}{2}\varepsilon_O(q_6)$	$\frac{1}{4} + 4\varepsilon_{Mz}(q_3,q_4) + 2\varepsilon_O(q_6)$
O8	$O4[T = \frac{1}{2}(b + c)]$	$\frac{1}{4}$	$\frac{3}{16} - \varepsilon_{Mz}(q_2) - \frac{1}{2}\varepsilon_O(q_6)$	$\frac{3}{4} - 4\varepsilon_{Mz}(q_2) + 2\varepsilon_O(q_6)$

above parameterization has nonetheless produced a very good approximation to rigid-body rotation of the AlO_4 and SiO_4 tetrahedra. Note, however, that there still remains the possibility of several alternative plausible starting models, *i.e.* while the magnitude of the parameters in Table 2 is known, their sign is not.

2.6. Alternative plausible starting models?

Given that there are several possible sign choices available for the four parameters listed in Table 2, it might be thought that there should be quite a few distinct possible plausible starting models, all of which would correspond to rigid-body rotation of the AlO_4 and SiO_4 tetrahedra. In fact there are only two distinct such models. Flipping the sign of the $q_6 = 0$ mode, *i.e.* flipping the sign of $\varepsilon_O(q_6)$ and switching Al and Si, does not generate a distinct starting model. Given that we make the choice that an Al atom is at the origin then $\varepsilon_O(q_6)$ must be positive and ~ 0.0056. We are free to choose the sign of $\varepsilon_{Mx}(q_1)$, as an origin shift of **b** (with respect to the original $C9$-related cell, see Fig. 3) is equivalent to flipping the sign of $\varepsilon_{Mx}(q_1)$, *i.e.* $2\pi q_1.\mathbf{b} = \pi$. Similarly the sign of $\varepsilon_{Mz}(q_2)$ can be chosen freely as an origin shift of $\frac{1}{2}(\mathbf{a} + \mathbf{c})$ is equivalent to flipping the sign of $\varepsilon_{Mz}(q_2)$ without affecting the sign of $\varepsilon_{Mx}(q_1)$, *i.e.* $2\pi q_2.\frac{1}{2}(\mathbf{a} + \mathbf{c}) = \pi$ whereas $2\pi q_1.\frac{1}{2}(\mathbf{a} + \mathbf{c}) = 0$. Having chosen the signs of $\varepsilon_{Mx}(q_1)$ and $\varepsilon_{Mz}(q_2)$, however, there still remains the sign of $\varepsilon_{Mz}(q_3,q_4)$ to be determined. These two distinct possible starting models (labelled models *A* and *B* from here on) will now be investigated *via* Rietveld refinement.

3. Constrained Rietveld refinement of low carnegieite

As explained in the *Introduction* an unconstrained Rietveld refinement of the crystal structure of low carnegieite using the previously published X-ray powder diffraction data (Thompson *et al.*, 1993) would not be feasible. In addition to the 48 displacive and eight compositional degrees of freedom there would also be a number of experimental parameters to be refined. The

Table 3. *Refinement statistics for the various model options*

Excluding data $20.5–22.2°$ and $55.2–75.7°$ 2θ. Parent Na's kicked off 0.01 of fractional coordinate. $R_p = 100\Sigma|y_i - y_{ci}|/\Sigma|y_i|$. $R_{wp} = 100[\Sigma w(y_i - y_{ci})^2]^{1/2}/\Sigma w y_i^2$. $R_{Bragg} = 100\Sigma|I - I_c|/\Sigma I$.

Model	R_p (%)	R_{wp} (%)	R_{Bragg} (%)
*A*12	5.2	7.2	6.3
*A*34	6.7	9.4	7.8
*A*14	9.6	13.2	8.0
*A*13	8.2	12.1	7.4
*A*23	10.7	14.5	9.8
*A*24	8.2	12.0	7.6
*A*1234	6.1	8.9	7.1
*B*12	8.4	12.0	8.2
*B*34	9.2	12.8	8.5
*B*1234	9.1	12.6	7.6

Coordinates of *A*12 Na's

	x	y	z
Na1	0.474	0.255	0.067
Na2	0.784	0.504	0.433

Table 4. *Apparent valences for starting models A and B, and for the final refined model*

Apparent valences calculated as the sums of bond valences for distances < 3.5 Å. R_o from *EUTAX*.

	Model *B*12*	Model *A*12*	Model *A*12	Refined model
Al1	3.07	3.07	3.07	3.06
Al2	3.07	3.07	3.07	3.06
Si1	4.04	4.04	4.04	4.06
Si2	4.04	4.04	4.04	4.05
Na1	1.01	1.01	0.97	0.91
Na2	1.01	1.01	0.91	0.94
O1	2.07	2.07	1.99	2.01
O2	1.97	1.97	2.10	2.03
O3	1.98	2.05	2.03	1.97
O4	2.05	2.05	1.98	2.06
O5	1.97	1.97	1.99	1.96
O6	2.07	2.07	1.94	1.99
O7	2.05	1.98	2.00	1.98
O8	1.98	1.98	1.98	1.97

* Na atoms in parent positions.

large unit cell observed for low carnegieite requires that, while there are a large number of reflections, these reflections are severely overlapping for most of the powder profile. In short, the data are not good enough to treat all the variables independently.

Table 5. *Atomic coordinates of starting models A and B, and the final refined model*

	Model B			Model A			Refined model*		
	x	y	z	x	y	z	x	y	z
Al1	0.9673	0.0000	0.9376	0.9673	0.0000	0.0624	0.966 (3)	0.000 (-)	0.067 (7)
Al2	0.2827	0.2500	0.5624	0.2827	0.2500	0.5624	0.282 (3)	0.254 (3)	0.559 (6)
Si1	0.2173	0.1250	0.0624	0.2173	0.1250	0.0624	0.216 (3)	0.129 (3)	0.064 (5)
Si2	0.9673	0.8750	0.4376	0.9673	0.8750	0.5624	0.968 (3)	0.875 (2)	0.563 (6)
Na1	0.5000	0.2500	0.0000	0.5000	0.2500	0.0000	0.475 (3)	0.250 (3)	0.051 (5)
Na2	0.7500	0.5000	0.5000	0.7500	0.5000	0.5000	0.773 (3)	0.507 (3)	0.456 (6)
Na3	0.7500	0.3750	0.0000	0.7500	0.3750	0.0000			
Na4	0.0000	0.6250	0.5000	0.0000	0.6250	0.5000			
O1	0.0652	0.0980	0.0000	0.0652	0.0980	0.0000	0.067 (2)	0.097 (2)	0.999 (8)
O2	0.4460	0.2826	0.5000	0.4460	0.2826	0.5000	0.446 (2)	0.280 (2)	0.502 (8)
O3	0.0000	0.9659	0.6140	0.0000	0.9035	0.8636	0.002 (5)	0.905 (2)	0.857 (4)
O4	0.2500	0.1535	0.3636	0.2500	0.1535	0.3636	0.249 (5)	0.153 (1)	0.363 (3)
O5	0.8040	0.0326	0.0000	0.8040	0.0326	0.0000	0.806 (2)	0.036 (1)	0.002 (9)
O6	0.1848	0.3480	0.5000	0.1848	0.3480	0.5000	0.183 (1)	0.352 (1)	0.503 (9)
O7	0.0000	0.9035	0.1364	0.0000	0.9659	0.3860	0.997 (4)	0.968 (2)	0.389 (3)
O8	0.2500	0.2159	0.8860	0.2500	0.2159	0.8860	0.246 (4)	0.217 (1)	0.877 (3)

* The errors were determined during the constrained refinement of all the atoms using I_{obs} extracted from the full powder profile. To convert fractional coordinates from the listed $Pb2_1a$ setting to the standard $Pca2_1$ setting: $(x, y, z)Pca2_1 = (x, z, -y)Pb2_1a$.

The derivation of the structural models for the aluminosilicate framework (models *A* and *B*) has been explained above. These models are necessarily chemically plausible, at least as far as the AV's of the Si—O and Al—O bond lengths and O—O distances are concerned. These two models do not give the Na-atom ordering. This has to be solved from the data and the positions subsequently refined.

Given that the stoichiometry required two Na atoms in four sites (see Table 2) there are six possible combinations with full occupancy of half the sites as well as the possibility of half occupancy of all the sites. It was considered necessary to test all these possible ordering patterns with both the framework models to determine which was the most likely structural model.

3.1. *Testing the models*

The program *DBW*3.2 (Wiles & Young, 1981) was used throughout for Rietveld analysis of the X-ray powder diffraction profile. Non-atomic parameters refined throughout were zero point, scale, peak profile and half-width using a pseudo-Voigt function, peak asymmetry and unit-cell dimensions. An overall temperature factor was also refined.

For each of the model/Na ordering combinations the Na-atom positional parameters (6 or 12) were refined simultaneously with 13 non-atom parameters. The background was interpolated between 14 points. Only data out to 55.2° 2θ (90 reflections) were used as it was considered that data at higher angles were too severely overlapping to be useful at this stage. The very strong 111$_{parent}$ reflections at ~21° 2θ were excluded from the refinement as they possessed a peculiar profile and were likely to be significantly off scale, both resulting from the method of data collection (see Thompson *et al.*, 1993). The final refinement statistics for each are presented in Table 3.

While all the combinations gave a moderately good fit to the data, there were three combinations which were significantly better than the rest, namely $A12$, $A34$ and $A1234$. On this basis we can immediately exclude model *B* for the aluminosilicate framework. Of the three Na combinations for model *A* it was clear that $A12$ was significantly better, ~1% lower in R_p than the next best model. On this basis we concluded that model *A* with full occupancy of Na1 and Na2 sites (see Table 2) was the best.

3.2. *Further refinement*

Having refined the Na-atom positions it was possible to test further the chemical plausibility of model *A* by calculation of AV's. These are presented together with the Na positions in Table 4. Apart from slight underbonding of the two Na atoms, model $A12$ with Na positions refined gave a remarkably good fit to the data even without further constrained refinement.

As *DBW*3.2 does not allow for bond-length constraints it was necessary to conduct constrained refinement of atoms external to the program. This was achieved by extracting I_{obs} from the Rietveld analysis with the $A12$ model with refined Na-atom positions. At this point it was considered appropriate to use the full profile, again except for the 111$_{parent}$ reflections at ~21° 2θ. The profile refinement statistics R_p and R_{wp} converged to 6.3 and 8.5% with a derived R_{Bragg} of 6.7%. These data were input into *SHELX*76 (Sheldrick, 1976), the weakest 30% of the extracted I_{obs} (64 of the 208 data) not being used because of their inherent unreliability.

Before refinement of the positional parameters, the 144 observed reflections gave an R_1 of 10.31%. By placing slack constraints on the Si—O and Al—O distances to be 1.624 ± 0.01 and 1.757 ± 0.01 Å, in accordance with the bond-valence requirement discussed earlier, the R_1 improved dramatically to 6.98%. The

Table 6. *Bond lengths* (Å) *and selected interatomic distances* (<3.6 Å)

Al1	Si1	3.14 (4)	3.21 (4)
	Si2	3.10 (4)	3.13 (4)
	O1	1.75 (3)	
	O3	1.76 (4)	
	O5	1.75 (4)	3.54 (4)
	O6		3.40 (4)
	O7	1.75 (4)	3.54 (4)
Al2	Si1	3.21 (5)	3.17 (5)
	Si2	3.08 (5)	3.14 (5)
	O2	1.75 (4)	3.48 (4)
	O3		3.43 (5)
	O4	1.77 (4)	
	O6	1.73 (4)	
	O8	1.76 (4)	3.57 (4)
Si1	O1	1.63 (4)	
	O4	1.61 (3)	
	O5	1.63 (4)	
	O8	1.60 (4)	
Si2	O2	1.63 (4)	
	O3	1.61 (4)	
	O6	1.62 (3)	
	O7	1.61 (4)	
Na1	O1	2.36 (5)*	
	O2	2.38 (5)*	2.88 (5)
	O3	2.41 (5)*	
	O4	3.13 (5)	
	O5	3.48 (4)	
	O6	3.45 (4)	
	O7	3.53 (5)	
	O8	2.56 (5)*	2.84 (5)
Na2	O1	3.49 (5)	3.13 (5)
	O3	3.16 (5)	
	O4	2.26 (4)*	
	O5	2.96 (5)	2.51 (5)*
	O6	2.37 (4)*	
	O7	2.85 (5)	2.55 (5)*
	O8	3.41 (4)	

Al1 tetrahedron			Al2 tetrahedron		
O1	O3	2.87 (4)	O2	O4	2.79 (5)
	O5	2.81 (3)		O6	2.88 (2)
	O7	2.80 (4)		O8	2.96 (4)
O3	O5	2.83 (5)	O4	O6	2.96 (3)
	O7	2.88 (3)		O8	2.80 (2)
O5	O7	2.96 (5)	O6	O8	2.78 (4)

Si1 tetrahedron			Si2 tetrahedron		
O1	O4	2.76 (5)	O2	O3	2.59 (4)
	O5	2.60 (3)		O6	2.63 (2)
	O8	2.57 (4)		O7	2.76 (4)
O4	O5	2.56 (4)	O3	O6	2.76 (5)
	O8	2.66 (2)		O7	2.57 (3)
O5	O8	2.69 (2)	O6	O7	2.52 (4)

* Approximately tetrahedral coordination of Na atoms by O atoms.

new O-atom positions gave a spread of O—O distances of 2.78-2.97 Å for AlO₄ tetrahedra and 2.54-2.77 Å for SiO₄ tetrahedra, compared with 2.80-2.98 Å and 2.58-2.78 Å for model *A*, respectively. Using these 're-fined' atomic positions in the Rietveld analysis lowered R_p, R_{wp} and R_{Bragg} to 5.7, 7.6 and 5.0%, respectively. The final positional parameters for this structural model are presented in Table 5 and the corresponding AV's in Table 4. Bond lengths and O—O distances are given in

Table 6.* As a result of extreme correlation between the profile background at higher angles and overall temperature factors it was arbitrary which was fixed at some meaningful value. Either way the present data contained no useful information about thermal motion. The refined unit-cell parameters were uniformly 0.1% larger than those determined previously from the Guinier data using an internal Si calibration standard, the difference being consistent with the effect of peak profile asymmetry.

Unconstrained refinement of the positional parameters both during the Rietveld analysis and using the extracted intensities in *SHELX*76 gave further improvement in the relevant refinement statistics. However, we concluded that this improvement in refinement statistics was a result of the increased degrees of freedom. In the Rietveld refinement there was severe correlation between some atomic parameters and non-atomic variables. As these unconstrained refinement models all gave AV's which were quite ridiculous it was decided that our constrained refinement was the best that could be achieved with the available data.

The observed, calculated and difference profiles, together with reflection markers are presented graphically in Fig. 7. The difference profile shows an inability of the Rietveld analysis to completely model the reflection profiles at low angle. This is probably as a result of the data being measured from a Guinier–Hagg film as described previously (Thompson *et al.*, 1993). Experience has shown that without a plausible starting model which already gives a reasonable fit to the profile, such as
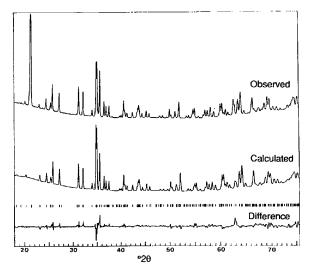
Fig. 7. The observed, calculated and difference profiles together with reflection markers for the final refined model.

our model $A12$, attempts to refine structures using such overlapping powder data leads to the situation where the refined model becomes completely dependent on the starting model. Our comparative testing of the various models, described earlier, helped us to avoid any such false refinement minima.

4. Summary and discussion

Like its octahedral corner-connected perovskite counterpart (Barnighausen, 1980), the $C9$ structure type represents an ideal parent structure or aristotype from which many lower symmetry derivative structures can be obtained *via* appropriate rotation of more or less rigid framework polyhedra (tetrahedral in the case of $C9$-related structures and octahedral in the case of perovskite-related structures). Given that one of the major objectives of crystal chemistry is the interrelationship between such cognate crystal structures, it is important not only to solve for the crystal structure of low carnegieite but also to place it in relationship to its underlying $C9$ aristotype. The use of a modulation wave approach to the structural parameterization and refinement of low carnegieite not only spelt out this relationship in detail but also made clear that there is more than one plausible starting model compatible with rigid-body rotation of the tetrahedral framework. Such an approach allowed for the systematic testing of alternative possibilities and hence avoided any problems associated with false refinement minima. It also provided plausible and essential starting models for the subsequent full Rietveld refinement.

Topologically the coupled tetrahedral edge rotations which generate the structure of low carnegieite from its underlying $C9$ aristotype have $Pbca$ space-group symmetry (for our choice of cell setting) and in this sense the structure of low carnegieite is closely related to those of $KGaO_2$ (Vielhaber & Hoppe, 1969) and $Na_{1-x}[Fe_{1-x}Si_x]O_2$ (Grey *et al.*, 1990). The major difference and the origin of the reduction in space group symmetry from $Pbca$ to $Pb2_1a$ in the case of low carnegieite arises from the difference in the ordering of the tetrahedral and stuffing cations. In the case of low carnegieite, the Al/Si and Na/vacancy ordering corresponds to a $q = 0$ compositional modulation of its underlying $C9$ aristotype whereas, in the case of $Na_{1-x}[Fe_{1-x}Si_x]O_2$, the Fe/Si and Na/vacancy ordering require a $q = b^*$ compositional modulation.

References

BARNIGHAUSEN, H. (1980). *Commun. Math. Chem.* **9**, 139–175.
BRADLEY, C. J. & CRACKNELL, A. P. (1972). *The Mathematical Theory of Symmetry in Solids*, p. 118. London: Oxford Univ. Press.
BRESE, N. E. & O'KEEFFE, M. (1991). *Acta Cryst.* **B47**, 192–197.
BROWN, I. D. & ALTERMATT, D. (1985). *Acta Cryst.* **B41**, 244–247.
FORIS, C. M., ZUMSTEG, F. C. & SHANNON, R. D. (1979). *J. Appl. Cryst.* **12**, 405–406.
GREY, I. E., HOSKINS, B. F. & MADSEN, I. C. (1990). *J. Solid State Chem.* **85**, 202–219.
KLINGENBERG, R. & FELSCHE, J. (1981). *J. Appl. Cryst.* **14**, 66–68.
O'KEEFFE, M. & HYDE, B. G. (1976). *Acta Cryst.* **B32**, 2923–2936.
PEREZ-MATO, J. M., MADARIAGA, G., ZUÑIGA, F. J. & GARCIA ARRIBAS, A. (1987). *Acta Cryst.* **A43**, 216–226.
SHANNON, R. D. (1979). *Phys. Chem. Miner.* **4**, 139–148.
SHELDRICK, G. M. (1976). *SHELX76. Program for crystal structure determination.* Univ. of Cambridge, England.
THOMPSON, J. G., WITHERS, R. L., WHITTAKER, A. K., TRAILL, R. M. & FITZ GERALD, J. D. (1993). *J. Solid State Chem.* In the press.
VIELHABER, E. V. & HOPPE, R. (1969). *Z. Anorg. Allg. Chem.* **369**, 14–32.
WILES, D. B. & YOUNG, R. A. (1981). *J. Appl. Cryst.* **14**, 149–151.
WITHERS, R. L., HUA, G. L., WELBERRY, T. R. & VINCENT, R. (1988). *J. Phys. C*, **21**, 309–318.
WITHERS, R. L., THOMPSON, J. G. & WELBERRY, T. R. (1989). *Phys. Chem. Miner.* **16**, 517–523.
WITHERS, R. L., WALLENBERG, R., BEVAN, D. J. M., THOMPSON, J. G. & HYDE, B. G. (1989). *J. Less Common Met.* **156**, 17–27.
YAMAMOTO, A. (1982). *Acta Cryst.* **A38**, 87–92.

Structure of Ba4Nb14O23

BY G. SVENSSON AND J. GRINS

Department of Inorganic Chemistry, Arrhenius Laboratory, Stockholm University, S-106 91 Stockholm, Sweden

Abstract

Single crystals of $Ba_4Nb_{14}O_{23}$ were obtained by heat treatment of a pelleted mixture of $Ba_5Nb_4O_{15}$, Nb_2O_5 and Nb at 1725 K in an Ar atmosphere. High-resolution electron microscopy studies showed the structure to be an intergrowth of the $BaNbO_3$ perovskite structure and the NbO structure. The structure model was refined using X-ray single-crystal diffraction data. Characteristic structural units are triple chains of corner-sharing Nb_6 octahedra, parallel to the c axis and separated by perovskite-type columns. Crystal data: barium oxoniobate, $Ba_4Nb_{14}O_{23}$, $M_r = 2218.0$, orthorhombic, *Cmmm*, $a = 20.79(1)$, $b =$